Drying Transition in the Hydrophobic Gate of the GLIC Channel Blocks Ion Conduction

Fangqiang Zhu[†*] and Gerhard Hummer[‡*]
[†]Department of Physics, Indiana University-Purdue University Indianapolis, Indianapolis, Indiana; and [‡]Laboratory of Chemical Physics, National Institute of Diabetes and Digestive and Kidney Diseases, National Institutes of Health, Bethesda, Maryland

ABSTRACT The theoretical prediction of water drying transitions near nonpolar surfaces has stimulated an intensive search for biological processes exploiting this extreme form of hydrophobicity. Here we quantitatively demonstrate that drying of a hydrophobic constriction is the major determinant of ion conductance in the GLIC pentameric ion channel. Molecular-dynamics simulations show that in the closed state, the channel conductance is ~12 orders-of-magnitude lower than in the open state. This large drop in conductance is remarkable because even in the functionally closed conformation the pore constriction remains wide enough for the passage of sodium ions, aided by a continuous bridge of ~12 water molecules. However, we find that the free energy cost of hydrating the hydrophobic gate is large, accounting almost entirely for the energetic barrier blocking ion passage. The free energies of transferring a sodium ion into a prehydrated gate in functionally closed and open states differ by only 1.2 kcal/mol, compared to an 11 kcal/mol difference in the costs of hydrating the hydrophobic gate. Conversely, ion desolvation effects play only minor roles in GLIC ion channel gating. Our simulations help rationalize experiments probing the gating kinetics of the nicotinic acetylcholine receptor in response to mutations of pore-lining residues. The molecular character and phase behavior of water should thus be included in quantitative descriptions of ion channel gating.

INTRODUCTION

The many unusual properties of water include a large sensitivity of its phase behavior to confinement. As a result, highly nonpolar surfaces may induce interfacial drying at ambient conditions (1). Confinement into volumes of molecular-scale dimensions can amplify this effect and cause water to recede entirely from hydrophobic enclosures (2–4). Theoretical studies of water in simple pores such as carbon nanotubes (5) and experiments on proteins (6,7) show that the resulting voids can constitute the thermodynamically favored state, challenging the view that nature abhors a vacuum. Molecular-scale drying of hydrophobic enclosures is thought to be exploited in a variety of biological functions (3,4). In a series of molecular-dynamics (MD) simulations, transient drying was observed in the formation of protein-protein complexes involving strongly hydrophobic interfaces (8). Enhanced affinities associated with drying have also been suggested for the binding of small ligands (9–11). Drying, modulated by the geometry and local polarity of the pore, has been implicated as a factor controlling the flow of protons in enzyme catalysis and biological energy transduction (4), with water chains forming the wires required for fast proton transport (12). But, most directly, drying of the pore in a membrane channel has been suggested as an effective gate blocking the transport of ions (13,14). Indeed, in MD simulations water was found to recede from hydrophobic constrictions not only in model systems (5,13) but also in several ion channels (15–20), supporting a possible role in ion channel gating.

But is such drying of an ion channel merely a side effect of the structural changes in the pore that is easily reverted as an ion enters, or does drying indeed account for the high energetic barrier associated with ion passage through a functionally closed membrane channel?

An early attempt to answer this question was made for the MscS channel (16), but the low cost of only ~3 kcal/mol for rehydration was based on a rough energetic model and on a channel structure that may not correspond to a functionally closed state (21,22). The functional importance of drying in channel gating thus remains unclear.

Here we perform a detailed calculation of the contribution of drying to the free energy barrier for cation passage through the GLIC ion channel (23), after showing that the structure corresponds to a functionally closed state. GLIC is a bacterial member of the large family of pentameric ligand-gated ion channels (24) that open or close in response to external signals such as ligand binding. The nicotinic acetylcholine receptor (nAChR) and other members of the family play important roles in neural signal transduction. Recent high-resolution structures of the close relatives GLIC and ELIC (25–27) have previously allowed us to monitor the gating transition at atomic resolution from an open to a closed state (18). We found that water receded completely from a ~15 Å-long segment of the closing channel in a single cooperative transition. To quantify the contribution of this drying transition to channel gating, we first confirm that the closed-state conformation of the GLIC channel indeed blocks ion conduction. We then calculate the free energy as a function of the sodium ion position and of the number of water molecules in the hydrophobic constriction. By comparing these free energies, we show that hydrating the hydrophobic

Submitted March 1, 2012, and accepted for publication June 4, 2012.

*Correspondence: fzhu0@iupui.edu or gerhard.hummer@nih.gov

Editor: Cynthia Czajkowski.

0006-3495/12/07/0219/9 $2.00

http://dx.doi.org/10.1016/j.bpj.2012.06.003

constriction of the channel, rather than the partial desolvation of the ion confined into the narrow pore, dominates the energetic barrier for ion passage in the functionally closed state. Our calculations directly and quantitatively demonstrate a possible functional role for drying in biology.

METHODS

Free energy of ion passage

We performed MD simulations of the transmembrane domain of GLIC embedded in a lipid bilayer and solvated by water molecules, resulting in a simulation system size of ~88,000 atoms. Details of the setup can be found in Zhu and Hummer (18). Specifically, to obtain the closed conformation of the protein, we started with the GLIC crystal structure and gradually directed the C_α atoms toward the corresponding positions in the ELIC crystal structure in a pulling MD simulation (18), followed by extensive equilibration (18). The backbone of the closed GLIC conformation used in this study is shown in Fig. 1, superimposed on the crystal structures of GLIC and ELIC.

The pore axis is aligned with the membrane-normal and points along the z axis. Restraints on selected C_α atoms (18) were applied to hold the pore in the closed or the open conformation in the respective simulations. To calculate the free energy profile $G(z)$ for the passage of a Na^+ ion through the GLIC pore, we extended our previous umbrella sampling simulations (18) (1 ns per window) and performed new simulations (2 ns per window) for both the open and the closed conformations. Simulations for each system involved 153 umbrella windows spaced at 0.5 Å distance along the z axis, covering a total distance of 76 Å between $z = \pm 38$ Å. In each umbrella window, the z-coordinate of the Na^+ ion was subject to a harmonic restraint with spring constant $K = 10$ kcal/(mol·Å^2). In the x-y dimensions parallel to the membrane, a flat-bottomed restraining potential $u(x,y)$ was applied,

$$u(x,y) = \begin{cases} 0 & \text{if } R \le R_0 \\ \dfrac{K\left[(x^2+y^2)^{1/2} - R_0\right]^2}{2} & \text{if } R > R_0, \end{cases} \quad (1)$$

with $R = (x^2 + y^2)^{1/2}$ and $R_0 = 7$ Å for the new simulations. We note that this lateral potential $u(x,y)$ will influence the offset of the corresponding free energy profile in the channel region (28). However, this effect can be properly taken into account in the calculation of ion occupancy and ion conductance, so that the results do not depend on the chosen lateral restraint (28). Moreover, the same lateral restraint is adopted in the simulations both of the open and of the closed conformations, and the difference between the calculated free energies is thus essentially independent of $u(x,y)$.

In these simulations, Hamiltonian replica exchange (29) was used to enhance the sampling efficiency, with attempts to swap conformations between neighboring umbrella windows every 200 fs. The last 1 ns of each simulation was used for analysis. Data from different umbrella windows were combined with the weighted histogram analysis method (30).

From the resulting free energy profiles $G(z)$ for ion passage along the pore axis, we calculated the probability of finding an ion in the pore segment. The average ion occupancy within the hydrophobic gate is

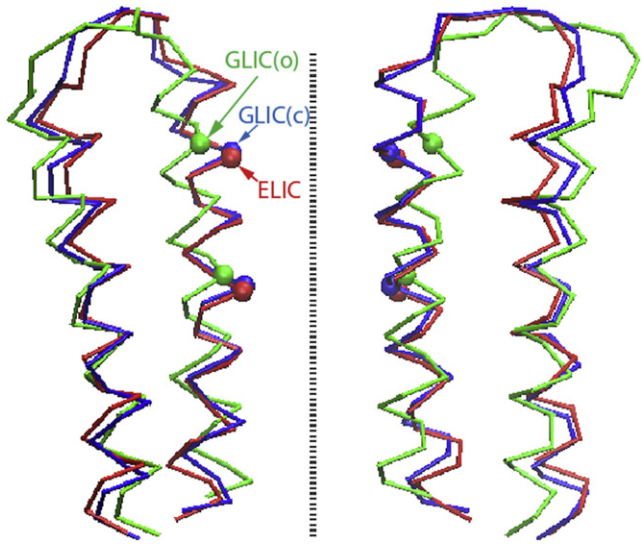

FIGURE 1 C_α traces of the M2 and M3 helices in the transmembrane domain. The crystal structures of ELIC (25), GLIC (26), and the computational model (18) of the closed GLIC channel in our simulations are superimposed. (*Dashed line*) Symmetry axis of the protein.

$$\langle N_{ion} \rangle = \rho S \int_{z_1}^{z_2} \exp[-\beta G(z)]dz,$$

with $\rho = 100$ mM used for the bulk ion density,

$$\beta = \frac{1}{k_B T},\ S = \iint dxdy \exp[-\beta u(x,y)],$$

and $G(z)$ shifted to have zero baselines in the bulk solvent, $|z| > \sim 35$ Å. Because $\langle N_{ion} \rangle << 1$, the gate is occupied by at most one ion. In this limit, $\langle N_{ion} \rangle = p_1$ is the probability of having exactly one ion in the pore, and $G_i = \beta^{-1} \ln[p_1/(1-p_1)] \approx -\beta^{-1} \ln \langle N_{ion} \rangle$ is the associated free energy of transferring an ion from the bulk into the gate region.

Free energy of water occupancy

To quantify the hydration state in the hydrophobic gate of the GLIC pore in the closed conformation, we employed a biased sampling of a coarse-grained water occupancy number $\widehat{N}$ (31,32). The hydrophobic region was defined as a cylinder along the z axis with a radius of 9 Å and a length of 14 Å between $z_1 = -3.7$ Å and $z_2 = 10.3$ Å. All water molecules in the pore with $z_1 \le z \le z_2$ were well within 9 Å of the pore axis and therefore inside the defined cylinder. We thus coarse-grained the pore water only in the z direction, defining the effective number of water molecules in the region of the hydrophobic gate as

$$\widehat{N} = \sum_i \int_{z_1}^{z_2} \widehat{\rho}_i(z)dz, \quad (2)$$

where the summation is over all water molecules that are within 9 Å of the pore center in the x-y plane and

$$\widehat{\rho}_i(z) = \begin{cases} \exp\left[-\dfrac{(z-z_i)^2}{2\sigma^2}\right] \Big/ \displaystyle\int_{-2\sigma}^{2\sigma} \exp\left(-\frac{z'^2}{2\sigma^2}\right)dz' & \text{if } |z-z_i| < 2\sigma \\ 0 & \text{if } |z-z_i| \ge 2\sigma \end{cases} \quad (3)$$

is the contribution of water molecule i with z-coordinate z_i to the occupancy number. The expression $\hat{p}_i(z)$ is a normalized Gaussian distribution truncated at 2σ, with $\sigma = 1$ Å, and effectively spreads the water density over a length of 4σ in the z-direction. With this definition, the water occupancy $\hat{N}$ becomes a continuous variable that may adopt noninteger values, and its probability distribution (or equivalently, free energy) accordingly becomes a continuous function. However, this continuous occupancy $\hat{N}$ is very closely correlated with the discrete occupancy N obtained by simple counting.

The coarse-graining of the water number makes it possible to apply restraints to bias the water occupancy (31,32). Here we adopted a harmonic restraint

$$U = \frac{K_w}{2}\left(\hat{N} - n_r\right)^2,$$

in which n_r is the reference water number. According to Eqs. 2 and 3, pore water molecules near z_1 or z_2 are subject to restraining forces in the z-direction. Starting with an empty pore in the closed conformation, we carried out a 4.2-ns simulation in which the target occupancy n_r was increased from 0.5 to 20.5 in steps of 1, thus gradually populating the hydrophobic gate with water molecules. Using the snapshots in this trajectory as initial coordinates, we performed umbrella sampling simulations in each of the 21 windows using biasing potentials with a spring constant $K_w =$ 2.5 kcal/mol. Each simulation was run for 1 ns, and the last 0.9 ns of each trajectory were taken to calculate the free energy $G(\hat{N})$ as a function of $\hat{N}$ using the weighted histogram analysis method (30).

We determined the free energy G_w of populating the pore in functionally open and closed states from the corresponding free energies $G(\hat{N})$. With an ion inside the hydrophobic gate of the closed pore, our MD simulations show a water occupancy of $\hat{N} \approx 12$ (Fig. 2 *c*). The probability of having 12 or more water molecules in the hydrophobic gate at equilibrium is

$$P_w\left(\hat{N} \geq 12\right) = \frac{\int_{\hat{N}=12}^{\infty} \exp\left[-\beta G\left(\hat{N}\right)\right] d\hat{N}}{\int_{\hat{N}=0}^{\infty} \exp\left[-\beta G\left(\hat{N}\right)\right] d\hat{N}},$$

and $G_w = -\beta^{-1} \ln P_w(\hat{N} \geq 12)$ is the corresponding free energy of hydrating the gate to this level.

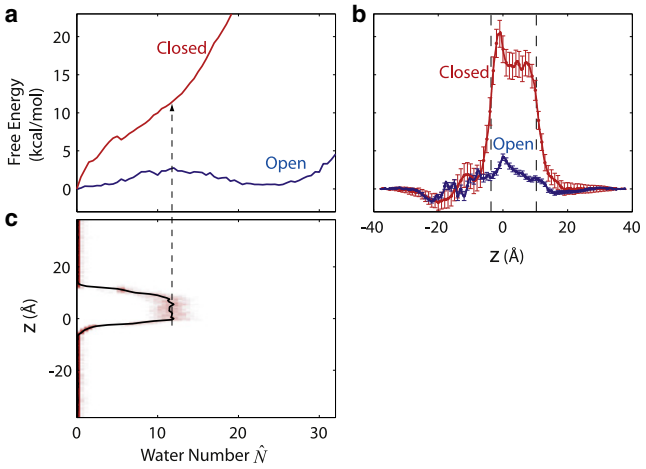

FIGURE 2 Free energy of hydration and ion translocation in GLIC. (*a*) Free energy $G(\hat{N})$ as a function of the coarse-grained water number $\hat{N}$ inside the hydrophobic gate. For the open conformation, the free energy $G(\hat{N}) = -k_BT \ln p(\hat{N})$ was obtained directly from the equilibrium probability distribution $p(\hat{N})$ in a 40-ns simulation (18). For the closed conformation, umbrella sampling was used (see Methods). (*b*) Free energy $G(z)$ as a function of the z-coordinate of a Na^+ ion, for the open and closed conformations. The extracellular side is at positive z values. (*Two vertical dashed lines*) Boundaries of the hydrophobic gate. (*c*) Probability distribution (*heat map*) and average (*solid curve*) of water occupancy $\hat{N}$ with a Na^+ ion restrained to different z-positions in closed-state simulations. (*Dashed arrow*) Plateau value $\hat{N} \approx 12$ when the ion is inside the hydrophobic gate.

RESULTS

Channel gating

How *closed* is the closed state of GLIC? Fig. 2 *b* shows the free energy profiles $G(z)$ for Na^+ passage through the GLIC transmembrane domain in the open and closed states. By combining umbrella sampling simulations with Hamiltonian replica exchange (29), we obtain a barrier for ion passage of almost 20 kcal/mol, which is remarkably high considering the fact that the pore does not pose a steric obstacle for ion passage. In contrast, the barrier in the open state is reduced to ~4 kcal/mol. This difference in barrier height implies a drop in conductance by a factor of $\sim\exp(-16\ \text{kcal/mol}/k_BT) \approx 10^{-12}$ at an ambient temperature $T = 300$ K, with k_B Boltzmann's constant. Given the open-state conductance of ~1 pS based on our calculations (18,28) and ~8 pS based on experiment (23), ion conduction through the pore in the closed conformation is thus effectively blocked.

Whereas the calculated ~20 kcal/mol free energy barrier for ion passage clearly shows that the channel in our simulations is functionally closed, we cannot entirely rule out that our structure differs from the closed-state structure of GLIC. Because the closed structure of GLIC has not been experimentally resolved, our closed-state model was derived by driving the C_α atoms from the backbone conformation in the GLIC crystal structure to that in the ELIC crystal structure, followed by extensive equilibration (18). A superimposition of the transmembrane domains (Fig. 1) shows that our closed-state GLIC model is much more similar to the ELIC crystal structure than to the GLIC crystal structure. For the C_α atoms in the five pore-lining M2 helices, our closed-state model has a root mean-square deviation (RMSD) of 0.9 Å to the ELIC crystal structure (25) and an RMSD of 3.1 Å to the GLIC crystal structure (26). In comparison, the RMSD for the M2 helices between the two crystal structures (25,26) is 3.0 Å.

Moreover, at the 9′ position (equivalent to Ile^{232} of GLIC), the distances of the C_α atom to the symmetry axis are 6.2 Å, 6.8 Å, and 7.6 Å in our closed-state model, ELIC, and GLIC crystal structures, respectively. At the 16′ position (equivalent to Ile^{239} of GLIC), the corresponding distances are 6.6 Å, 6.9 Å, and 9.8 Å. Therefore, at the

backbone level, our closed-state model is slightly narrower in the hydrophobic constriction than the ELIC crystal structure, and considerably narrower than the GLIC crystal structure. When side chains are considered, however, ELIC exhibits a narrower constriction than our closed-state GLIC model, mainly due to the bulky phenylalanine side chains at the 16′ position in ELIC. Although the C_α radius at 9′ is slightly smaller than at 16′ (see data above) in the ELIC crystal structure, the narrowest constriction is actually formed by the Phe side chains at 16′ (25). In contrast, in GLIC both 9′ and 16′ positions feature an Ile residue, and the constriction (~1.7 Å in radius, with side chains included) formed by Ile^{232} at 9′ is thus slightly narrower than that formed by Ile^{239} at 16′ in the closed conformation (18), consistent with the C_α radii above.

The MD simulations also allow us to monitor the hydration of the pore in the absence and presence of the Na^+ ion. In our previous study (18) we found that in the absence of an ion, the hydrophobic gate between the two Ile rings, Ile^{232} and Ile^{239}, exhibited fluctuations between water-filled and empty states in the open conformation, but remained completely empty with the pore in the functionally closed conformation. In contrast, here we find that when the Na^+ ion is near or inside the hydrophobic gate, the region is always fully hydrated, consistent with earlier findings for the MscS channel (16). Snapshots of the pore region in the absence and presence of Na^+ are shown in Fig. 3. Ion passage thus induces rehydration of the pore, even in the functionally closed conformation of the channel. This complete reversal of the drying transition of the pore induced by an approaching ion (Fig. 2 *c*) might suggest that the high barrier for ion passage is simply a consequence of the partial desolvation of the ion in the narrow pore. Drying of the pore would then be relegated to a mere side effect, without any significant contribution to ion channel gating.

Gate hydration

To quantify the contribution of drying, we determine the equilibrium free energy of hydrating the pore. For the open conformation, this free energy can be determined directly from the 40-ns equilibrium simulation in our previous study (18), which showed multiple transitions between the water-filled and empty states. In the open conformation, the free energy profile $G(\widehat{N})$ as a function of the coarse-grained water occupancy $\widehat{N}$ in the hydrophobic gate (Fig. 2 *a*, and see Methods, above) represents a bimodal distribution with two metastable states: an empty state at $\widehat{N} \approx 0$, and a filled state at $\widehat{N} \approx 22$.

For the closed channel, water filling of the hydrophobic gate did not occur in a 40-ns equilibrium simulation (18). Here we thus carry out umbrella sampling simulations to determine the free energy of hydrating the pore at equilibrium. The resulting closed-state $G(\widehat{N})$ overall increases monotonically with $\widehat{N}$, indicating the absence of a metastable filled state (Fig. 2 *a*). A minor dip of $G(\widehat{N})$ at $\widehat{N} \approx 5.5$ corresponds to the connection of two broken water chains entering at opposite ends of the hydrophobic gate to form a continuous and bridging H-bonded chain. The steep rise in the closed-state $G(\widehat{N})$ implies that the filling of the gate in the closed conformation is energetically highly unfavorable.

From the free energies $G(\widehat{N})$ for the closed state of the pore, we find that the cost of hydrating the pore without ion is large. With an ion inside the hydrophobic gate of the closed pore, our MD simulations show a water occupancy of $\widehat{N} \approx 12$ (Fig. 2 *c*). The free energy cost of hydrating the pore to this level in the absence of an ion is $G_w \approx 11.4$ kcal/mol (see Methods). For comparison, the free energy cost of transferring an ion into the gate region is $G_i = 15.3$ kcal/mol at physiological salt concentrations of ~100 mM, as determined by integration of $G(z)$ (see Methods). The free energy cost G_w of hydrating the pore in the absence of an ion thus amounts to three-quarters of the overall cost G_i of ion transfer into the gate. This large contribution demonstrates that drying of the pore, not desolvation of the ion or its direct electrostatic interactions with the channel, is the main factor determining the high barrier for ion passage.

Except for this hydration penalty, the free energy difference for ion transfer into open and closed pores is

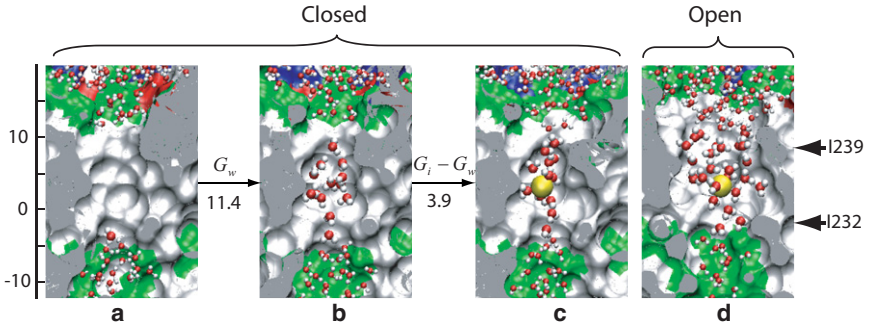

FIGURE 3 Snapshots of cuts through the GLIC pore interior, with the extracellular side up. Water molecules within and immediately outside the hydrophobic gate region are shown (51). (*Arrows* on the *right*) Approximate positions of the Ile^{232} and Ile^{239} rings. Free energy differences between the states are given in kcal/mol. (*a*) Closed conformation without restraint on the water number or ion position (18). (*b*) Closed conformation with a water occupancy of $\widehat{N} \approx 12$, corresponding to the average value of $\widehat{N}$ when an ion is restrained to the center of the gate region. (*c*) Closed conformation with a Na^+ ion restrained to the gate region. (*d*) Open conformation with a Na^+ ion restrained to the gate region.

remarkably small. In the closed conformation, the free energy difference between an ion in the properly hydrated pore and in the bulk solvent is $\Delta G = G_i - G_w = 3.9$ kcal/mol (at 100 mM bulk salt concentration). The corresponding difference of $\Delta G = 2.7$ kcal/mol for the channel in the open conformation is only slightly smaller, with $G_i = 3.1$ kcal/mol from the open-state $G(z)$ and $G_w = 0.4$ kcal/mol from $G(\widehat{N})$ (Fig. 2 and Table 1). On the basis of these results, the free energies of the ion in the hydrated gates of functionally open and closed states differ by merely 1.2 kcal/mol. Therefore, it is almost entirely the difference of 11 kcal/mol in the hydration costs G_w that is responsible for the dramatic drop in the ion occupancy and conductance upon channel closing.

Interaction range

Because drying dominates the barrier for ion passage, yet an approaching ion invariably hydrates the hydrophobic constriction, one may ask where in the channel the effective force resulting from drying acts on the ion to block its passage, and how this repulsive force is coupled to changes in the gate hydration state. In Fig. 4 we compare the free energy profile $G(z)$ as a function of the ion position to the average water occupancy $\widehat{N}(z)$. In the closed conformation of the channel, the highest free energies are found when the ion is inside the hydrophobic gate, coincident with the peak hydration level in this region. At both boundaries of the hydrophobic gate, the ion experiences a steep rise in the free energy. These sharp increases in the potential of mean force $G(z)$ cause large but short-ranged average repulsive forces on the approaching ion. Roughly at the same locations, the water occupancy inside the gate also undergoes sharp transitions from the empty to the filled state.

When approached from the extracellular side ($z > 0$), the increase in the free energy coincides almost exactly with the increase in the average number of water molecules; from the intracellular side ($z < 0$), the rising edge in $G(z)$ is shifted toward the left by a short distance relative to that in $\widehat{N}(z)$. This small displacement between the two curves and the narrow peak in $G(z)$ at $z \approx -1$ Å followed by a plateau between 0 and ~8 Å indicate that when the ion approaches from $z < 0$, full hydration of the gate is induced only after the ion has crossed its narrowest part at $z \approx -1$ Å. By forcing the ion, on average, through a dry constriction, the energetic barrier is increased, explaining the peak in $G(z)$ at $z \approx -1$ Å; with the gate hydrated after passage of the narrowest part of the channel, no further energetic penalty is incurred, explaining the plateau. Overall, we conclude from Fig. 4 that the repulsion of the ion from the dry hydrophobic constriction acts at short range, on a length scale comparable to the size of a water molecule. Consistent with this short-range repulsion, there is no significant penalty for the ion to enter the channel regions just above and below the constriction, even in the functionally closed conformation.

TABLE 1 Free energy of hydrating the gate in the functionally open and closed states of GLIC, and of transferring the Na^+ ion from the bulk phase (with 100 mM salt concentration) into the gate

Free energy [kcal/mol]	Open	Closed
G_w (hydrating pore)	0.4	11.4
G_i (transfer Na^+ into pore)	3.1	15.3
$G_i - G_w$ (transfer Na^+ into prehydrated pore)	2.7	3.9

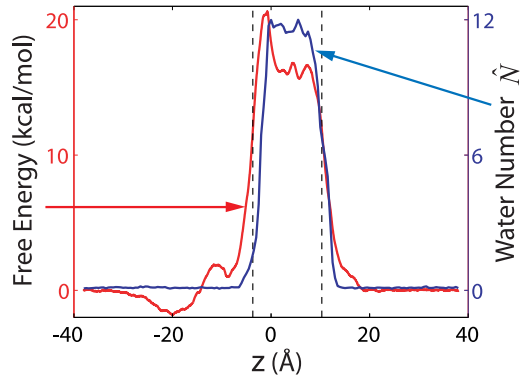

FIGURE 4 Free energy $G(z)$ of the ion (*left scale*) and the average water occupancy (*right scale*) as a function of the ion position for the closed conformation, as in Fig. 2, *b* and *c*, respectively.

DISCUSSION

Mechanism of ion blockage

Although our closed conformation of GLIC behaved very stably in our simulations (18) and appears to be a reasonable model for the closed state, it is conceivable that the model does not fully capture all features of the conformation due to artifacts such as the absence of the extracellular domain. We thus do not rule out the possibility that the GLIC channel in the closed state may have even narrower constrictions at the hydrophobic gate than in our model, possibly with an even higher free energy barrier for ion passage. Nonetheless, our calculations show that the open and closed models adopted here already exhibit a dramatic difference in ion conductance, and that our closed-state model corresponds to a nonconducting channel. On the basis of our calculations it is therefore safe to conclude that drying is sufficient for a functional closing of the channel.

Undoubtedly, some protein channels may adopt a closed state in which the pore is so narrow that ion passage can be sterically blocked, e.g., at the constriction formed by $Phe^{16'}$ of ELIC (25), as discussed in Results. Not surprisingly, simulations show that the hydrophobic region of ELIC is completely empty of water (20). However, even when the constriction becomes wider so that ion or water could potentially pass through without steric clashes, the pore may repel

water and ions due to its hydrophobic nature. Indeed, when $Phe^{16'}$ in ELIC was mutated into an alanine (33), the ELIC structure remained essentially the same except for the elimination of the steric constriction, but still resulted in a nonconducting state (33). When the hydrophobic constriction exceeds a certain radius, a water-filled state of the pore will emerge (a mechanism known as "hydrophobic gating" (13)), and only in such a state can ions possibly be conducted. We note that under normal temperatures the geometry of the pore is expected to be dynamic, due to thermal fluctuations and the flexibility of protein structures, and there thus may not always be a clear boundary between the regimes of steric and hydrophobic gating.

Water model and membrane potential

Possible inaccuracies in the MD force fields are another concern, in particular our use of a simple water model. In the channel hydration equilibrium, errors in the chemical potential of water in the reference bulk phase are extensive, i.e., proportional to the occupancy number of water molecules (4). For TIP3P water, the excess chemical potential is ~0.2 kcal/mol less negative than that of real water (34), with a negligible contribution coming from bulk density differences. On the basis of this difference, the free energy penalty for rehydration of the hydrophobic gate with $\widehat{N} \approx 12$ real water molecules would actually be ~2.4 kcal/mol higher, thus further increasing the importance of drying. Corrections for possible force-field issues are thus not likely to eliminate the role of drying in the gating process.

An electric potential across the membrane should also affect the hydration equilibrium of the hydrophobic gate. On the basis of simulations for single-file water (34), we would expect that the interactions of water with an external electric field of ~0.1 V/nm would lower the free energy penalty for filling with $\widehat{N} \approx 12$ water molecules by ~1 kcal/mol. Biological membrane potentials would thus not be sufficient to induce filling of the hydrophobic constriction.

Dielectric continuum models

Previously, valuable insights were obtained from continuum dielectric models (35), in which ion channels provide high-dielectric connections through the low-dielectric hydrocarbon core of the membranes. In particular, continuum calculations indicate a high energy cost to bring an ion into a small water-filled cavity in a low-dielectric medium (35,36). To stabilize the ion in the interior of the channel, such energy must be compensated by a highly favorable electrostatic environment provided by the protein (36). Although protein electrostatics is not the focus of this study, we note that it is incorporated in MD simulations and plays a major role in the obtained ion potentials of mean force, as reflected by the large difference between the Na^+ and Cl^- potentials of mean force from atomic simulations of GLIC (37,38).

Moreover, the protein electrostatic environment is not expected to be very sensitive to small conformational changes. Because the open- and closed conformations are overall quite similar, as in the crystal structures (25–27), the long-range protein electrostatics affects both states in a similar manner. In contrast, hydrophobic gating is highly sensitive to the pore size and, as found here, a relatively small change in the pore radius may give rise to a large change in ion conductance. Therefore, gated ion channels not only provide a favorable environment to the conducted ion to make its passage possible, but may also employ hydrophobic gating to sharply switch the pore between the open and closed ion-conducting states.

For the highly heterogeneous GLIC channel, it is not quite feasible to assign uniform dielectric constants as in simple models (35). In contrast, atomic simulations effectively capture such electrostatic effects without making explicit assumptions about the dielectric constant, and thus extend the continuum theories with significantly more detailed descriptions, in particular, with an explicit account of the molecular character of water. In classical force fields, each atom has a fixed partial charge for the electrostatic interactions, and dielectric screening is reproduced mainly through orientation polarization (e.g., of water dipoles) in response to the local electric field. MD simulations adopting the classical force fields have achieved remarkable success in reproducing the free energy and conduction rate in ion channels (19,39). Nonetheless, incorporation of higher-order quantum-mechanical effects, such as atomic polarizability, would in principle further improve the accuracy of the simulations, at the expense of increased computational cost.

Ion selectivity

Whereas hydrophobic constrictions provide a sensitive and relatively simple mechanism for channel gating, such constrictions are generally not responsible for ion selectivity. Discrimination between different ion species typically involves direct and strong interactions of ions with hydrophilic groups of the channel, as seen for instance in the selectivity filter of the K^+ channels (40,41). GLIC and other pentameric ligand-gated ion channels selectively conduct cations over anions, but impose little discrimination between different cations such as Na^+ and K^+. Ion selectivity in these channels is normally attributed to some glutamate residues at the intracellular entrance. MD simulations (37,38) showed that Cl^- ions indeed experience much higher free energy barriers in GLIC and thus cannot be conducted.

Experimental validation

In correspondence to Le Chatelier's principle, the large difference in the energetic costs of drying the open and

closed channels should affect the channel gating equilibrium between open and closed states (42). The hydrophobicity of the GLIC gate mainly originates from the pore-facing residues Ile^{232}, Ala^{236}, and Ile^{239}. Interestingly, when the counterpart of Ala^{236} in nAChR, a valine residue, was mutated into hydrophilic amino acids, the equilibrium constant of nAChR was shifted toward the open state by 3–4 orders of magnitude (43,44). Remarkably, a sterically conservative mutation of valine to asparagine produced the most pronounced shift among all mutations in the ε-subunit of nAChR, and the largest change in the α-subunit was also produced by mutating the corresponding residue into a threonine (43,44). Flanked by rings of bulky residues, these valine mutants are not expected to significantly affect the geometry of the pore. It thus appears likely that the hydration state may at least partially account for this dramatic shift in the equilibrium between open and closed conformations. With a more hydrophilic character of the mutants, the cost of dehydrating the pore upon channel closure increases; in turn, enhanced attractive interactions with water help stabilize the open state of the channel.

Our simulation results also shed some light on the measured effects of mutations on the opening and closing rates. Jha et al. (44) used these kinetic measurements in a Φ-value analysis to determine the sequence of events in nAChR channel opening when bound to an agonist. Residues with low Φ-values were interpreted as experiencing a late change in their local environment during the closed-to-open transition (43,44). In the asparagine mutant, closing was slowed down ~160 times, whereas opening sped up only ~30 times, consistent with the hypothesis that the more hydrophilic channel is less easily dehydrated. We note further, that the important role of hydration for channel conduction also explains the low Φ-values (44) measured for some pore-facing residues at the hydrophobic gate, as the gate would remain dry until the channel is almost fully open on the basis of our MD simulations here and in Zhu and Hummer (18). Overall, the results of the experiments by Purohit et al. (43) and Jha et al. (44) on the closely related nAChR channel are consistent with an energetically and mechanistically important role of drying in GLIC channel gating.

Although dewetting is repeatedly observed in MD simulations of ion channels and water appears to play a role in the observed ionic current between hydrophobic surfaces (45), experimental verification of dewetting in ion channels is still highly desired. Lacking direct evidence from experiment, the question of dewetting remains open. With current experimental techniques, it is difficult to directly measure water occupancy in functional ion channels. In principle, the drying mechanism proposed here could be tested experimentally by varying the water activity. Whereas our calculations for the closed state suggest a strong bias toward a dry channel that is not easily reverted by increased water activity, the open state of GLIC is close to the midpoint in the wet-dry equilibrium, and this equilibrium should thus be sensitive to water activity changes. The water activity can be reduced by adding osmolytes excluded from the pore, and increased by applying hydrostatic pressure.

Assuming that there are no other significant effects on the channel and membrane, changes in water activity should be directly reflected in the open-state conductance of the wild-type GLIC channels, and possibly the open-closed equilibrium (43,44). Specifically, at higher osmolyte concentrations the hydrated state of the pore would have smaller probability, resulting in reduced conductance. In contrast, if wetting were unimportant, changes would be fully accounted for by differences in the free energy of ion solvation in the bulk phase. To probe such water activity effects also in the functionally closed state, mutations with hydrophilic residues in the hydrophobic gate could be used (43,44). We expect that such mutations shift the equilibrium toward the wet pore, even in the closed state.

Experimental measurements on nAChR showed that the single-channel conductance of nAChR is essentially independent of hydrostatic pressure up to 60 MPa (46). We note that the pore in the crystal structure of nAChR (47), generally believed to represent the closed conformation, is considerably wider than the ELIC crystal structure or the closed-state GLIC structure here. The open-state pore of nAChR, with a significantly larger single-channel conductance than GLIC, is also expected to be wider than the GLIC pore in the open conformation. It thus appears highly likely that the nAChR pore in the open-state is already predominantly filled with water at normal pressure, and further increasing the pressure would therefore introduce little effect. However, it would be interesting to perform pressure studies on GLIC, because volume contributions from ligand binding, conformational changes, and hydration effects (46) may be more easily separable for a proton-gated channel.

Moreover, the hydration state could possibly be inferred from water permeability measurements. If a channel is filled with a continuous column of water molecules, water may cross the channel from one side of the membrane to the other. Such water permeation could be detected by measuring the exchange rate of isotopically labeled water, or the net water transport rate under a driving force such as an osmotic pressure. Water permeability of some ion channels was indeed measured in experiments (48). For channels with hydrophobic gates, previous computational studies and our calculations here indicate a strong correlation between ion conduction and water permeation. In the open state, GLIC and ELIC should exhibit substantial water permeability, even without the presence of permeant ions and an applied voltage. In the closed state, in contrast, due to the high hydration free energy, our results predict no water permeation as well. Moreover, for the GLIC channel in the closed state, we show here that the introduction of a Na^+ ion into the hydrophobic gate would rehydrate the

gate. Similar rehydration appears likely if charged groups are covalently linked to Ala^{236}, thus mimicking the electrostatics of an ion, and the modified channel might then have detectable water permeability even in the closed state. Combined studies by simulations and experiments are required to verify such predictions.

Finally, we note that the focus of this study is on the closed state of GLIC and on the mechanism of sodium ion blockage in this state. Properties of the open state offer more opportunities to validate simulations by experiments, in which the single-channel conductance can be measured. In our recent study (28), we demonstrated that the single-channel conductance can also be calculated from atomic simulations. In future studies it is thus desirable to repeat such calculations (28) in simulations with different permeant ions, channel mutants, solvent environments, or temperatures (49), and to further evaluate our computational models by comparing the calculated conductance with experimental measurements.

CONCLUSIONS

We showed that drying of the hydrophobic gate accounts for a large fraction of the energetic barrier for ion passage through the GLIC channel. Because our findings are consistent with experiments reported for the nAChR channel, and because drying has already been observed in simulations of several channels (15–18), we expect that the important functional role for drying demonstrated here is not unique to GLIC. The textbook model of ion permeation through biological membranes (35) should thus be extended to account for the drying-induced barrier. The magnitude of the drying contribution to the barrier obtained here implies that one can no longer ignore the molecular character of water and its unusual phase properties in descriptions of ion-channel gating.

With the precaution that the extent and physical characteristics of drying at protein surfaces remain contentious (50) due to the lack of direct experimental verification, our results provide supporting evidence for drying transitions in protein pores and quantify their role in an important biological function, the control of ion conduction through membrane channels. Experimental studies, such as those suggested here, are highly desired to test the theories and to shed light on this intriguing issue.

This research was supported by the Intramural Research Programs of The National Institute of Diabetes and Digestive and Kidney Diseases, National Institutes of Health and utilized the high-performance computational capabilities of the Biowulf Linux cluster at the National Institutes of Health, Bethesda, Maryland (http://biowulf.nih.gov).

REFERENCES

1. Chandler, D. 2005. Interfaces and the driving force of hydrophobic assembly. *Nature.* 437:640–647.
2. Wallqvist, A., and B. J. Berne. 1995. Computer-simulation of hydrophobic hydration forces on stacked plates at short-range. *J. Phys. Chem.* 99:2893–2899.
3. Berne, B. J., J. D. Weeks, and R. Zhou. 2009. Dewetting and hydrophobic interaction in physical and biological systems. *Annu. Rev. Phys. Chem.* 60:85–103.
4. Rasaiah, J. C., S. Garde, and G. Hummer. 2008. Water in nonpolar confinement: from nanotubes to proteins and beyond. *Annu. Rev. Phys. Chem.* 59:713–740.
5. Hummer, G., J. C. Rasaiah, and J. P. Noworyta. 2001. Water conduction through the hydrophobic channel of a carbon nanotube. *Nature.* 414:188–190.
6. Collins, M. D., G. Hummer, …, S. M. Gruner. 2005. Cooperative water filling of a nonpolar protein cavity observed by high-pressure crystallography and simulation. *Proc. Natl. Acad. Sci. USA.* 102:16668–16671.
7. Qvist, J., M. Davidovic, …, B. Halle. 2008. A dry ligand-binding cavity in a solvated protein. *Proc. Natl. Acad. Sci. USA.* 105:6296–6301.
8. Liu, P., X. Huang, …, B. J. Berne. 2005. Observation of a dewetting transition in the collapse of the melittin tetramer. *Nature.* 437:159–162.
9. Abel, R., T. Young, …, R. A. Friesner. 2008. Role of the active-site solvent in the thermodynamics of factor Xa ligand binding. *J. Am. Chem. Soc.* 130:2817–2831.
10. Baron, R., P. Setny, and J. A. McCammon. 2010. Water in cavity-ligand recognition. *J. Am. Chem. Soc.* 132:12091–12097.
11. Brannigan, G., D. N. LeBard, …, M. L. Klein. 2010. Multiple binding sites for the general anesthetic isoflurane identified in the nicotinic acetylcholine receptor transmembrane domain. *Proc. Natl. Acad. Sci. USA.* 107:14122–14127.
12. Pomès, R., and B. Roux. 2002. Molecular mechanism of H^+ conduction in the single-file water chain of the gramicidin channel. *Biophys. J.* 82:2304–2316.
13. Beckstein, O., P. C. Biggin, and M. S. P. Sansom. 2001. A hydrophobic gating mechanism for nanopores. *J. Phys. Chem. B.* 105:12902–12905.
14. Roth, R., D. Gillespie, …, R. E. Eisenberg. 2008. Bubbles, gating, and anesthetics in ion channels. *Biophys. J.* 94:4282–4298.
15. Sotomayor, M., and K. Schulten. 2004. Molecular dynamics study of gating in the mechanosensitive channel of small conductance MscS. *Biophys. J.* 87:3050–3065.
16. Anishkin, A., and S. Sukharev. 2004. Water dynamics and dewetting transitions in the small mechanosensitive channel MscS. *Biophys. J.* 86:2883–2895.
17. Nury, H., F. Poitevin, …, M. Baaden. 2010. One-microsecond molecular dynamics simulation of channel gating in a nicotinic receptor homologue. *Proc. Natl. Acad. Sci. USA.* 107:6275–6280.
18. Zhu, F., and G. Hummer. 2010. Pore opening and closing of a pentameric ligand-gated ion channel. *Proc. Natl. Acad. Sci. USA.* 107:19814–19819.
19. Jensen, M. O., D. W. Borhani, …, D. E. Shaw. 2010. Principles of conduction and hydrophobic gating in K^+ channels. *Proc. Natl. Acad. Sci. USA.* 107:5833–5838.
20. Cheng, X., I. Ivanov, …, J. A. McCammon. 2009. Molecular-dynamics simulations of ELIC-a prokaryotic homologue of the nicotinic acetylcholine receptor. *Biophys. J.* 96:4502–4513.
21. Spronk, S. A., D. E. Elmore, and D. A. Dougherty. 2006. Voltage-dependent hydration and conduction properties of the hydrophobic pore of the mechanosensitive channel of small conductance. *Biophys. J.* 90:3555–3569.
22. Vásquez, V., M. Sotomayor, …, E. Perozo. 2008. A structural mechanism for MscS gating in lipid bilayers. *Science.* 321:1210–1214.
23. Bocquet, N., L. Prado de Carvalho, …, P. J. Corringer. 2007. A prokaryotic proton-gated ion channel from the nicotinic acetylcholine receptor family. *Nature.* 445:116–119.
24. Sine, S. M., and A. G. Engel. 2006. Recent advances in Cys-loop receptor structure and function. *Nature.* 440:448–455.

25. Hilf, R. J., and R. Dutzler. 2008. X-ray structure of a prokaryotic pentameric ligand-gated ion channel. *Nature.* 452:375–379.

26. Hilf, R. J., and R. Dutzler. 2009. Structure of a potentially open state of a proton-activated pentameric ligand-gated ion channel. *Nature.* 457:115–118.

27. Bocquet, N., H. Nury, …, P. J. Corringer. 2009. X-ray structure of a pentameric ligand-gated ion channel in an apparently open conformation. *Nature.* 457:111–114.

28. Zhu, F., and G. Hummer. 2012. Theory and simulation of ion conduction in the pentameric GLIC channel. *J. Chem. Theory Comput.* 10.1021/ct2009279.

29. Fukunishi, H., O. Watanabe, and S. Takada. 2002. On the Hamiltonian replica exchange method for efficient sampling of biomolecular systems: application to protein structure prediction. *J. Chem. Phys.* 116:9058–9067.

30. Kumar, S., D. Bouzida, …, J. M. Rosenberg. 1992. The weighted histogram analysis method for free-energy calculations on biomolecules. 1. The method. *J. Comput. Chem.* 13:1011–1021.

31. Patel, A. J., P. Varilly, and D. Chandler. 2010. Fluctuations of water near extended hydrophobic and hydrophilic surfaces. *J. Phys. Chem. B.* 114:1632–1637.

32. Andreev, S., D. Reichman, and G. Hummer. 2005. Effect of flexibility on hydrophobic behavior of nanotube water channels. *J. Chem. Phys.* 123:194502.

33. Zimmermann, I., and R. Dutzler. 2011. Ligand activation of the prokaryotic pentameric ligand-gated ion channel ELIC. *PLoS Biol.* 9:e1001101.

34. Vaitheeswaran, S., J. C. Rasaiah, and G. Hummer. 2004. Electric field and temperature effects on water in the narrow nonpolar pores of carbon nanotubes. *J. Chem. Phys.* 121:7955–7965.

35. Parsegian, A. 1969. Energy of an ion crossing a low dielectric membrane: solutions to four relevant electrostatic problems. *Nature.* 221:844–846.

36. Roux, B., and R. MacKinnon. 1999. The cavity and pore helices in the KcsA K^+ channel: electrostatic stabilization of monovalent cations. *Science.* 285:100–102.

37. Cheng, M. H., R. D. Coalson, and P. Tang. 2010. Molecular dynamics and Brownian dynamics investigation of ion permeation and anesthetic halothane effects on a proton-gated ion channel. *J. Am. Chem. Soc.* 132:16442–16449.

38. Fritsch, S., I. Ivanov, …, X. Cheng. 2011. Ion selectivity mechanism in a bacterial pentameric ligand-gated ion channel. *Biophys. J.* 100: 390–398.

39. Bernèche, S., and B. Roux. 2001. Energetics of ion conduction through the K^+ channel. *Nature.* 414:73–77.

40. Varma, S., D. M. Rogers, …, S. B. Rempe. 2011. Perspectives on: ion selectivity: design principles for K^+ selectivity in membrane transport. *J. Gen. Physiol.* 137:479–488.

41. Roux, B., S. Bernèche, …, H. Yu. 2011. Ion selectivity in channels and transporters. *J. Gen. Physiol.* 137:415–426.

42. Finkelstein, A. V., and E. I. Shakhnovich. 1989. Theory of cooperative transitions in protein molecules. II. Phase diagram for a protein molecule in solution. *Biopolymers.* 28:1681–1694.

43. Purohit, P., A. Mitra, and A. Auerbach. 2007. A stepwise mechanism for acetylcholine receptor channel gating. *Nature.* 446:930–933.

44. Jha, A., P. Purohit, and A. Auerbach. 2009. Energy and structure of the M2 helix in acetylcholine receptor-channel gating. *Biophys. J.* 96:4075–4084.

45. Sachs, F., and F. Qin. 1993. Gated, ion-selective channels observed with patch pipettes in the absence of membranes: novel properties of a gigaseal. *Biophys. J.* 65:1101–1107.

46. Heinemann, S. H., W. Stühmer, and F. Conti. 1987. Single acetylcholine receptor channel currents recorded at high hydrostatic pressures. *Proc. Natl. Acad. Sci. USA.* 84:3229–3233.

47. Unwin, N. 2005. Refined structure of the nicotinic acetylcholine receptor at 4Å resolution. *J. Mol. Biol.* 346:967–989.

48. Pohl, P., and S. M. Saparov. 2000. Solvent drag across gramicidin channels demonstrated by microelectrodes. *Biophys. J.* 78:2426–2434.

49. Gupta, S., and A. Auerbach. 2011. Temperature dependence of acetylcholine receptor channels activated by different agonists. *Biophys. J.* 100:895–903.

50. Giovambattista, N., C. F. Lopez, …, P. G. Debenedetti. 2008. Hydrophobicity of protein surfaces: separating geometry from chemistry. *Proc. Natl. Acad. Sci. USA.* 105:2274–2279.

51. Humphrey, W., A. Dalke, and K. Schulten. 1996. VMD: visual molecular dynamics. *J. Mol. Graph.* 14:33–38, 27–28.